# Morphological Development in Solvent-Cast Polystyrene−Polybutadiene−Polystyrene (SBS) Triblock Copolymer Thin Films

**G. Kim and M. Libera***

*Department of Materials Science and Engineering, Stevens Institute of Technology, Hoboken, New Jersey 07030*

*Received September 12, 1997; Revised Manuscript Received February 5, 1998*

ABSTRACT: This paper describes morphological development in solvent-cast polystyrene (PS)−polybutadiene (PB)−polystyrene (SBS) triblock copolymer thin films (30 wt % PS) as a function of solvent evaporation rate and post-evaporation annealing. Films were cast onto NaCl substrates to a thickness of order 100 nm. Plan-view and cross-sectional measurements by transmission electron microscopy show that the equilibrium morphology of in-plane cylinders is generated when films are given relatively long exposure to high solvent concentration or to elevated temperature. Alternate and metastable morphologies are generated under kinetically constrained conditions. Fast evaporation (∼200 nL/s) produces a microphase-separated microstructure with no long-range order. Intermediate evaporation (∼5 nL/s) generates hexagonally packed (vertical) PS cylinders in a PB matrix with the cylinder axis perpendicular to the film plane. Slow evaporation (∼1.5 nL/s) leads to a duplex microstructure of PS cylinders with domains of either vertical or in-plane cylinders. Post-evaporation annealing of films supported by a Cu TEM grid (18 h, 140 °C) converts the duplex morphology into one with only in-plane PS cylinders. Very slow solvent evaporation (∼0.2 nL/s) produces a fully in-plane cylinder microstructure. A distortion of the hexagonal PS array in the as-cast in-plane structure suggests that the as-cast block copolymer is affected by anisotropic deswelling during the final stages of solvent evaporation.

## Introduction

Block copolymers present a rich variety of microphase-separated morphologies depending on the polymer species involved, the molecular weight, the average composition, and the thermotropic/lyotropic processing characteristics. Block copolymers have been the subject of a number of reviews describing both theory and experiment.[1−3] A characteristic feature of block copolymer systems is the repulsion between unlike blocks, which leads to microphase separation at mesoscopic length scales. In perhaps the most commonly studied copolymer system, namely polystyrene−polydiene diblocks, the various equilibrium morphologies as a function of composition are fairly well established.[4−9] Minor-component compositions ranging from 0 to 20 wt % lead to spheres of the minor phase ordered on a cubic lattice in a continuous major-phase matrix. Minor-component compositions ranging from about 20 to 35 wt % produce minor-phase cylinders (rods) arranged on a hexagonal lattice in a continuous major-phase matrix. Minor-component compositions greater than 35 wt % lead to a morphology of alternating lamellae. In polystyrene (PS)−polyisoprene (PI) diblock copolymers, an ordered bicontinuous double-diamond morphology has been observed in specimens with PI composition of approximately 33 wt %,[10,11] and a gyroid morphology has been observed for a PI-37%PS diblock.[12]

Much of the research examining equilibrium block-copolymer morphologies has employed long annealing times under vacuum using relatively large specimens with characteristic dimensions ranging from tens of micrometers to several millimeters. These conditions minimize surface-thermodynamic effects, remove volatile solvents, and maximize the probability of a given specimen achieving its thermodynamic equilibrium morphology. Increasingly, research has concentrated on the evolution of microstructure and transformations between various phases in response to temperature, solvent, or shear.[13−17] Because of their use as compatibilizers[18,19] and adhesives[20] as well as their potential use as templates in lithographic applications,[21−24] there is a growing literature addressing both surface and kinetic effects on microphase separation where significant departures from the bulk equilibrium morphologies can be observed.

Kinetic and surface effects in thin-film copolymer specimens can constrain the bulk morphology away from the surface itself. In particular, the relative orientation of a microphase-separated morphology with respect to a surface can be changed as a function of specimen thickness, solvent evaporation rate, and annealing conditions, among other possible variables. This issue is of little concern to bulk equilibrium studies where the average properties of thick specimens can be studied by small-angle scattering methods or by thin sectioning from random locations in the bulk. However, the relative morphological orientation is of substantial significance in templating and diffusion-barrier applications. For example, Henkee et al.[25] used TEM to study the morphology of thin-film PS−PB copolymer droplets as a function of composition and showed that, depending on their composition and thickness, films can be terraced in order to maintain periodicity of the minor-phase spheres, cylinders, or lamellae. In a similar set of polymers, Mansky et al.[21,22] cast thin films of PS/PB diblocks to generate microphase-separated morphologies where the minor component aligns itself perpendicular to the film plane. Radzilowski et al.[26] used cross-sectional TEM to study the thickness effects on the morphology of post-cast annealed PS−PB diblock copolymer thin films and found that the thicker regions of a PB major copolymer film show a PS in-plane

S0024-9297(97)01349-1 CCC: $15.00 
Published on Web 03/31/1998

cylinder morphology. However, the minimum thickness region (25−27 nm) has a different morphology consisting of a PS interlayer penetrated by a hexagonal array of circular PB channels that connect upper and lower PB surface layers.

This paper explores kinetic effects associated with microphase separation in thin (∼100 nm) solvent-cast (toluene) films of 30 wt % PS PS−PB−PS (SBS) triblock copolymer. The effects of solvent evaporation rate, with evaporation times ranging from minutes to days, and post-evaporation annealing are examined. The morphology observed under conditions of slow solvent evaporation plus post-evaporation annealing consists of PS cylinders arranged in a hexagonal array with the cylinder axis aligned in the plane of the thin film. This would be expected as the "equilibrium" structure.[3,27] Films synthesized under constrained kinetic conditions lead to a logical progression of metastable microstructures which vary from (i) a disordered microphase-separated morphology at the fastest solvent evaporation rate to (ii) a vertical-cylinder morphology at intermediate rates, (iii) a duplex vertical/in-plane cylinder morphology at slower rates, and finally (iv) a fully in-plane cylinder morphology at the slowest evaporation rates. Post-evaporation annealing can either coarsen an as-cast microstructure or transform it to a more stable one. TEM examination of cross-sectional specimens confirms that films formed under kinetically constrained conditions can have metastable bulk morphologies.

## Experimental Procedure

Thin-film specimens of SBS triblock copolymer were prepared by solution casting from toluene. SBS was purchased from Scientific Polymer Products, Inc. Characterization by gel permeation chromatography (GPC) and proton NMR determined that this polymer was 30 wt % polystyrene with $M_w$ = 112 000 and contained small amounts (≤5%) PS/PB diblock and PS homopolymer. On the basis of the GPC data, the polydispersity was estimated to be 1.02. The polymer was dissolved in toluene to produce a 0.1 wt % solution. Then ∼50 $\mu$L of solution was deposited on a water-polished NaCl single-crystal substrate, with lateral dimensions of about 1 cm by 1 cm, contained in a small evaporation dish. The solvent evaporation rate could be controlled by adding toluene drops to the dish around, but not on, the substrate and by covering or partially covering the dish. The evaporation rate was estimated using the ratio of the total initial volume of solution to the time to form a viable film as determined by visual inspection. Four qualitatively different solvent evaporation rates were studied. The fastest evaporation rate corresponded to unrestricted evaporation of the solvent into air over a period of approximately 4 min producing a rate of ∼200 nL/s. An intermediate evaporation rate was generated by covering the dish, leaving only a small hole for solvent vapor to escape. Under these conditions, the casting process occurred over approximately 3 h corresponding to a rate of ∼5 nL/s. A slow evaporation rate (∼1.5 nL/s) was generated by completely covering the dish. Under these conditions, solvent could only escape through the small gap between the dish and its cover, and evaporation was complete after approximately 10 h. Finally, a very slow evaporation condition was achieved by sealing the dish and its cover using a textile gasket. Evaporation was complete after approximately 3 days, generating a ∼0.2 nL/s evaporation rate.

After solvent evaporation, each thin film was cut into small squares on its salt substrate using a razor blade. These were floated from the substrate in water, and each square was collected on a copper TEM grid. Some specimens were subjected to a post-cast annealing treatment at 140 °C, higher than $T_g$ (∼100 °C) of polystyrene, for 18 h under a vacuum of $10^{-6}$ Torr after being mounted on a Cu TEM grid. Early annealing experiments were done under a vacuum of $10^{-2}$ Torr with little obvious difference in the resulting microstructure. Typical specimens contained many grid squares (∼10−20) of electron-transparent film with a thickness of approximately 100 nm. Within a given specimen, some thickness variations were observed with a minority fraction of grid squares containing film too thick for useful 300 keV electron transmission.

Each film was stained by exposure for 20 min to $OsO_4$ vapor from $OsO_4$ crystal warmed to 50 °C. $OsO_4$ reacts preferentially with the unsaturated carbon double bond in the polybutadiene block. Its higher Coulombic potential produces more high-angle electron scattering, so the stained polybutadiene phase appears dark in a bright-field TEM image. In all micrographs presented here, the PB phase appears dark and the PS phase appears light.

Cross-sectional TEM specimens of various SBS films were prepared by a sequence of steps. After observing a film's morphology in plan view, a thin carbon layer was evaporated on both sides of the stained film on its TEM grid. The specimen was then embedded in epoxy and subsequently cured at room temperature. Cross-sectional specimens were cut using a Reichert-Jung cryo-ultramicrotome with the specimen at −110 °C. This temperature is below the $T_g$ of PB (∼ −90 °C). Microtomed sections were collected either on Cu TEM grids or on holey carbon TEM grids.

Transmission electron microscopy was done on a Philips CM30 Super Twin TEM and a Philips CM20 FEG TEM/STEM. The CM30 is a 300 keV instrument with a thermionic $LaB_6$ electron source and tilt limited to ±12°. The CM20 is a 200 keV instrument with a Schottky field emission electron source and tilting capabilities of ±60°. Quantitative image analysis was done on (i) digital images scanned from negatives and prints or (ii) digital images collected directly from the CM20 microscope using a Gatan multiscan camera system. The analysis procedure used the Gatan digital micrograph software. The reciprocal-space length scale associated with Fourier transformed images was calibrated using digital high-resolution images of single-crystal silicon.

## Results

The effect of solvent evaporation rate on the diene-rich SBS thin film morphology is described by Figure 1. The insets show Fourier transforms from representative portions of each image. Fast-evaporation conditions (∼200 nL/s) generate a highly disordered microstructure (Figure 1a) with evidence of microphase separation but with no long-range order. The intermediate evaporation rate (∼5 nL/s) produces a highly ordered microphase-separated morphology (Figure 1b) consisting of polystyrene cylinders arranged in a hexagonal array within a continuous polybutadiene matrix. The axis of each cylinder is perpendicular to the plane of the polymer thin film. This morphology will be referred to as the vertical-cylinder structure. The slow evaporation rate (∼1.5 nL/s) generates a duplex morphology containing PS cylinders in a PB matrix (Figure 1c) where there are regions extending laterally over many tens of microns with the vertical-cylinder morphology as well as regions with an in-plane PS cylinder morphology where the axes of the PS cylinders lie in the film plane. The very slow solvent evaporation condition (∼0.2 nL/s) produces a morphology made up entirely of in-plane PS cylinders (Figure 1d).

The effect of post-evaporation annealing is illustrated by Figure 2. Annealing the disordered microphase-separated structure resulting from fast evaporation (Figure 1a) coarsens that structure. While one can find local regions that suggest an incipient ordering, annealing does not convert the overall morphology into one with a dramatically different or more symmetric mor-

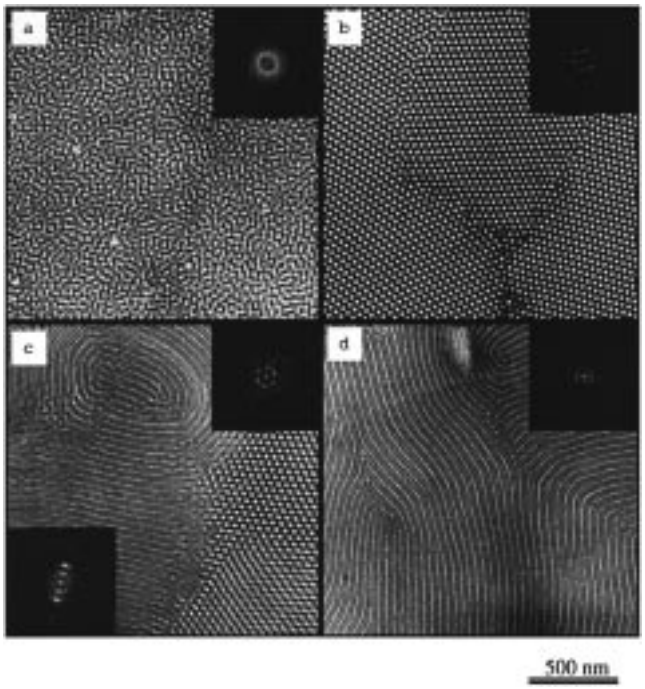


**Figure 1.** Plan-view bright-field TEM images of the as-cast $OsO_4$-stained SBS thin films with inset Fourier transforms: (a) fast (∼200 nL/s); (b) intermediate (∼5 nL/s); (c) slow (∼1.5 nL/s); (d) very slow (∼0.2 nL/s).

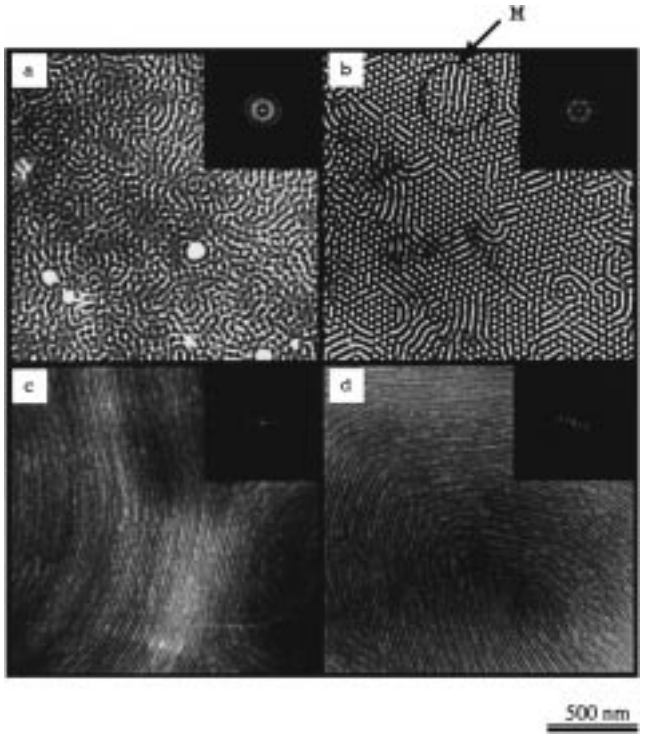


**Figure 2.** Plan-view bright-field TEM images of the as-cast $OsO_4$-stained SBS thin films subjected to post-evaporation annealing for 18 h. at 140 °C with inset Fourier transforms: (a) fast (∼200 nL/s); (b) intermediate (∼5 nL/s); (c) slow (∼1.5 nL/s); (d) very slow (∼0.2 nL/s).

phology (Figure 2a). Annealing the hexagonally arrayed vertical-cylinder morphology (Figure 1b) generated by the intermediate evaporation conditions partially converts the vertical-cylinder morphology to include modified regions (labeled "M") having features of light contrast elongated in the film plane (Figure 2b). The overall morphology remains predominantly one of hexagonally packed PS cylinders in a continuous PB matrix. Post-evaporation annealing of the duplex morphology characteristic of the slow evaporation conditions (Figure 1c) converts this morphology into a fully in-plane one (Figure 2c). Finally, annealing of films cast under very slow evaporation conditions (Figure 1d) slightly coarsens the in-plane cylinder morphology and reduces the overall contrast in the TEM images.

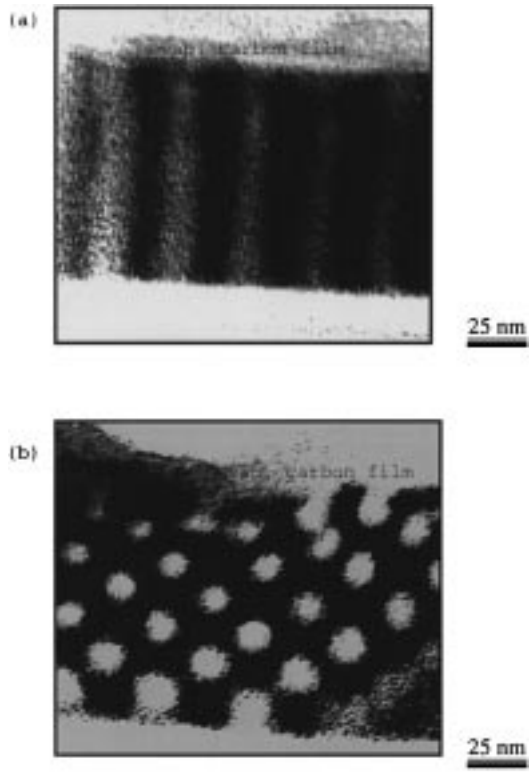


**Figure 3.** Bright-field TEM images of cross sections from $OsO_4$-stained films having the (a) vertical cylinder (intermediate rate) and (b) in-plane cylinder (very slow rate) morphologies.

Cross-sectional views provide further confirmation of the morphological nature of these thin films. Figure 3a shows a cross-sectional image from a specimen cast under the intermediate evaporation rate condition (Figure 1b). The film thickness is approximately 110 nm. This image clearly shows that the polystyrene cylinders are aligned approximately perpendicular to the plane of the film. In contrast, Figure 3b shows a cross sectional view of a film cast under the very slow evaporation-rate condition (Figure 1d). The film thickness is about 100 nm. This image shows polystyrene cylinders aligned end-on, confirming that the cylinders lie in the plane of the film.

Two types of microstructural anisotropies have been observed in the as-cast films. The first is an artifact. It is manifested by the Fourier transforms of plan-view images of as-cast films (Figure 1 insets). For example, the Fourier transform characteristic of the disordered microphase-separated microstructure (Figure 1a) is slightly elliptical. Similarly, the hexagonal pattern in the transform from the vertical-cylinder morphology (Figure 1b) shows interplanar angles slightly distorted from 60°. Such distortions have been observed to varying degrees in a number of as-cast films and are often small or negligible. These distortions are absent in the annealed films (Figure 2 insets). This category of distortion is attributed to anisotropic in-plane stretch-

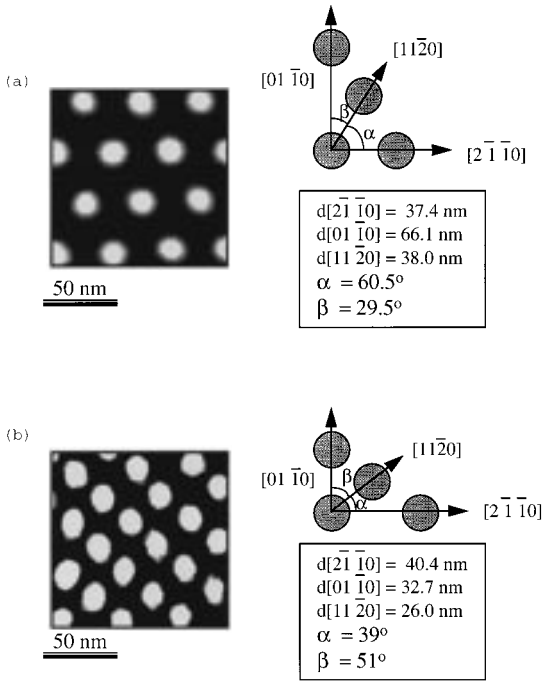


**Figure 4.** (a) Plan-view image of an as-cast film with the vertical-cylinder morphology and a schematic indicating a well-ordered hexagonal lattice. (b) Cross-sectional image of a relatively thick as-cast film (~300 nm) with the in-plane cylinder morphology and a schematic indicating a distorted hexagonal lattice.

ing of the film during specimen preparation. The as-cast films are floated from salt substrates onto water and collected on the Cu TEM support grid. This collection procedure and the subsequent drying could introduce such an in-plane anisotropy. The annealing process is applied to films already supported on a grid. The annealing is apparently sufficient for relaxation of small in-plane strains such that the in-plane distortion disappears and no new distortions are introduced.

The second microstructural anisotropy occurs perpendicular to the film plane and, as will be discussed later, is attributed to anisotropic deswelling of the PB matrix during the final stages of solvent evaporation. Illustrative data are shown in Figure 4. Figure 4a shows a plan-view image of an as-cast film with the vertical-cylinder morphology. The PS cylinders are arranged on a well-ordered hexagonal lattice. The schematic shows that the intercylinder spacing, $d^V$, is 37.4 nm and the characteristic angles (e.g., $\alpha^V$) are essentially 60°. In contrast, Figure 4b shows a cross-sectional image of a relatively thick (~300 nm) as-cast film with the in-plane cylinder morphology. In this image, the intercylinder spacing varies with orientation: $d^I_{[2,\bar{1},\bar{1},0]} \neq d^I_{[0,1,\bar{1},0]} \neq d^I_{[1,1,\bar{2},0]}$. The characteristic angles are not all the same, and $\alpha^I = 39°$ which is substantially smaller than the equilibrium 60° angle. This distortion has been observed repeatedly in a variety of both thick and thin as-cast in-plane cylinder films.

The response of the interdomain spacing to post-cast annealing is addressed by the characteristic spacing derived from Fourier transformed image data. Table 1 summarizes interdomain spacings typical of the as-cast and annealed morphologies generated from the various solvent-evaporation rates. Differences between the spacings associated with the four solvent-evaporation rates need further clarification because of the effects of morphology, cylinder orientation, and anisotropic deswelling. These will be discussed later. However, for a given solvent-evaporation rate, in all cases the interdomain spacing increases in response to post-cast annealing.

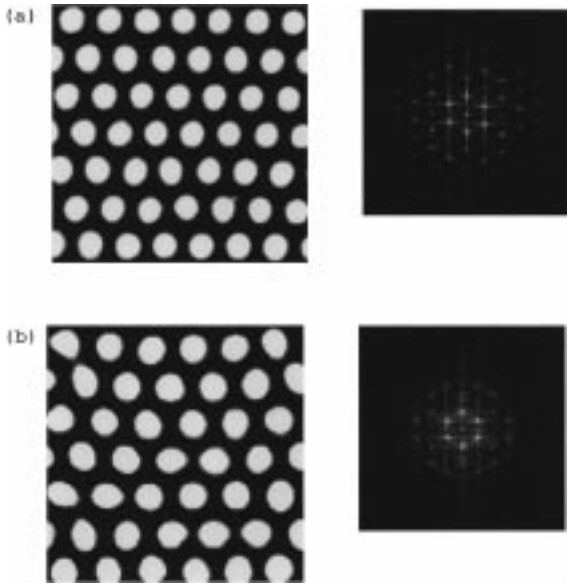


**Figure 5.** Plan-view bright-field images of 240 nm × 240 nm areas from films prepared under the intermediate evaporation rate in the (a) as-cast and (b) post-cast annealed states with Fourier transforms.

**Table 1. Interdomain Spacing from Fourier Transforms Derived from Images Characterizing the As-Cast and Post-Cast Annealed Structures (Figures 1 and 2, Respectively)**

| | fast evap (200 nL/s) $d$ (nm) | intermed evap (~5 nL/s) $d^V_{[2,\bar{1},\bar{1},0]}$ | slow (~1.5 nL/s) $d^V_{[2,\bar{1},\bar{1},0]}$ | slow (~1.5 nL/s) $d^I_{[2,\bar{1},\bar{1},0]}$ | very slow (0.2 nL/s) $d^I_{[2,\bar{1},\bar{1},0]}$ |
|---|---|---|---|---|---|
| as-cast | 36.7 | 36.9 | 39.7 | 41.5 | 44.5 |
| annealed | 43.2 | 40.8 | | 52.4 | 52.7 |

The combined changes in the interdomain spacing, $d$, and the PS cylinder radius, $r$, due to annealing can be studied for the particular case of the vertical-cylinder morphology. This morphology lends itself well to an experimental determination of the area fraction of each phase. Figure 5 shows a 240 nm × 240 nm area from films prepared under the intermediate evaporation rate in the (i) as-cast and (ii) post-cast annealed states. Figure 5a, from the as-cast state, comes from a sample which everywhere has the vertical-cylinder morphology. Figure 5b, from the annealed state, comes from a portion of sample which displays only a vertical-cylinder morphology and avoids portions with the modified morphology ("M" in Figure 2b). The area fraction of each phase was established by thresholding the digital image, so pixels with an intensity below the mean value were converted to pure white (intensity = 0) and pixels with an intensity above that value were converted to pure black (intensity = 255 on an 8-bit gray scale). Histograms of contrast characterizing these images are clearly bimodal. Identifying an appropriate threshold criterion is not difficult, and the resulting area fractions are relatively insensitive to variations in the thresholding criterion. The average pixel intensity from the resulting two-tone image can be directly converted into a measure of the area fraction of each phase.[28] The intercylinder spacing can be determined from Fourier transforms of the image data. The cylinder radius can be measured directly from the real-space images or

**Table 2. Effects of Annealing on the Vertical-Cylinder Morphology**

| specimen | intercylinder spacing $d$ (nm) | cylinder radius $r$ (nm) | PB area fraction |
|---|---|---|---|
| as-cast | 35.6 | 10.5 | 0.317 |
| annealed | 39.3 | 11.6 | 0.314 |

computed from the relation $r^2 = A_f d^2/0.866\pi$ knowing the area fraction $A_f$ of the PS phase and $d$. Analysis of Figure 5 is summarized by Table 2. Annealing increases both $r$ and $d$ while maintaining $A_f$ approximately constant.

## Discussion

**(i) Equilibrium Bulk Morphology.** There is already experimental evidence in the literature using bulk specimens and long annealing times that the equilibrium morphology of SBS triblock copolymer with a composition of 30 wt % PS consists of PS cylinders in a PB matrix.[29] This result is also predicted theoretically.[27] Under the least-constrained conditions studied in this research, namely the very slow evaporation rate (~0.2 nL/s) coupled with post-evaporation annealing, a microstructure of PS cylinders is generated in films approximately 100 nm thick. Given even more time and temperature for continued diffusional rearrangement, the film would presumably thicken in response to surface-energy effects.

The in-plane cylinder morphology can be distinguished from a vertical-lamellar morphology in two ways. The first is the direct approach of simply studying these films in cross section. Figure 3b shows a cross-sectional TEM image of one such film where there is an array of disks with light contrast in a continuous matrix of dark contrast. These disks correspond to PS cylinders viewed end-on lying in the plane of the film. A vertical-lamellar microstructure would have bands of light contrast running through the thickness of the film depending on the viewing direction.

A second and somewhat more elegant approach to understand the contrast observed in plan-view images uses simulations assuming different microstructural models. TEM images of films produced, for example, under very slow evaporation conditions (Figure 1d) show a highly reproducible pattern of contrast alternating periodically between light, dark, and gray as one follows a $[2,\bar{1},\bar{1},0]$ direction. Figure 6a shows a high-magnification view of one-such area where the lines of contrast are all parallel. Figure 6b shows a horizontal intensity profile of this image taken from the rectangular box in Figure 6a. The profile is averaged over many pixels vertically to improve the signal-to-noise ratio. There are three important features in this profile: (i) there are two maxima, one more intense the other; (ii) the curves in the vicinity of the maxima are everywhere concave downward; (iii) the maxima are separated by regions of uniform low contrast. These characteristics are observed in simulated images of an in-plane morphology observed in plan view. Figure 7a illustrates schematically the model specimen assumed for simulation. It consists of rows of PS cylinders lying in the film plane with PB surface layers. The number of rows, the cylinder radius, and the spacing between cylinders can be easily varied. A kinematic electron-scattering approximation based on mass-thickness differences is used where $OsO_4$-stained PB is assumed to scatter strongly and unstained PS weakly. Figure 7b shows a plan-view

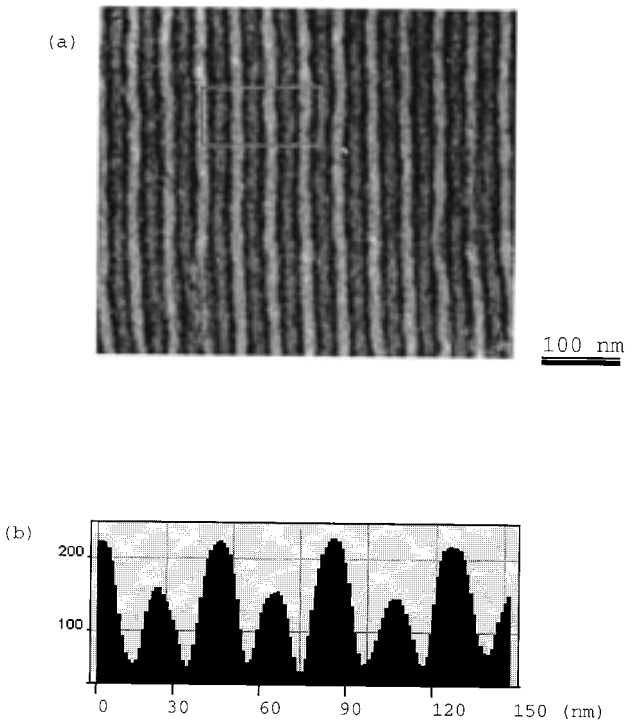


**Figure 6.** (a) Plan-view bright-field TEM image of an $OsO_4$-stained film produced by very slow solvent evaporation showing parallel contrast variations characteristic of the in-plane cylinder morphology. (b) Profile of intensity as a function of lateral position averaged vertically over the rectangular box indicated in part a.

image derived from a specimen with the cross-sectional structure of Figure 7a (7 PS rows; PS cylinder radius = 10 nm; PS cylinder spacing = 35 nm). Parallel lines of alternating light, dark, and gray contrast are observed. The line profile of Figure 7c shows the same features as the experimental image (Figure 6). Varying the parameters in the calculation does not change the general characteristics of this line profile. Quantitative agreement between the simulated and experimental images would demand better definition of the number of PS rows in the experimental film and a more accurate model for the differential electron scattering.

**(ii) Metastable Bulk Morphologies.** The various microphase-separated morphologies observed are a clear function of the time the various films are exposed to elevated solvent concentrations or to elevated temperatures. Elevated solvent concentration and temperature both increase the diffusivities of the polymer components in this thin-film system. Given enough time under conditions of relatively high diffusivity, the films will adopt their thermodynamically stable state. Less time effectively freezes in some metastable microstructure.

Parts a−d of Figure 1 show a clear progression in the resultant morphology as a function of solvent evaporation rate. The fastest evaporation rate (Figure 1a) generates a solid polymer film over a time scale of just a few minutes. While no long-range order is present, microdomains with light and dark contrast are clearly evident, indicating that this polymer has had time to locally phase separate into PB-rich and PS-rich microdomains. Insufficient time under conditions of high polymer mobility is available to further transform the chaotic structure into one with long-range translational order. A similar phenomenon was observed by Harkless

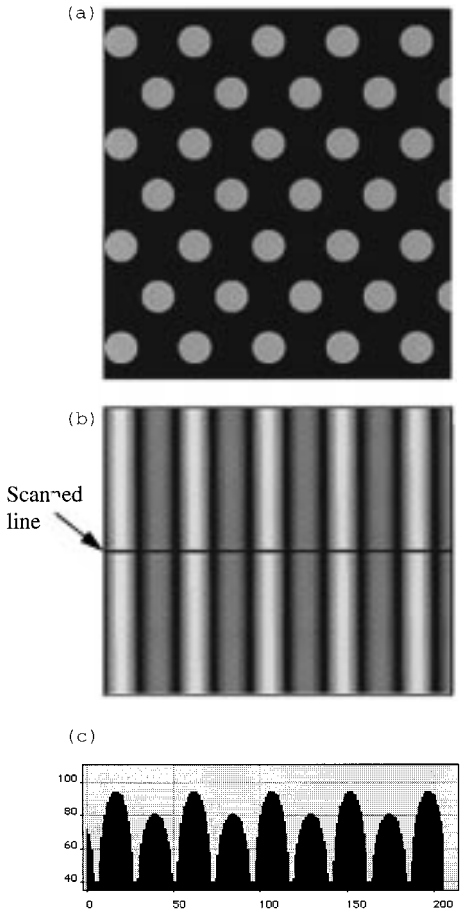


**Figure 7.** Kinematic scattering model from a specimen with in-plane PS cylinder morphology illustrated in cross section by part a predicting a plan-view image shown in part b, which leads to a lateral intensity profile shown in part c.

et al.[14] using time-dependent X-ray scattering to monitor the development of microstructure in the PS−PB diblock after quenching from a temperature above the ordering temperature. Their scattering data indicate that microphase-separated domains form with no long range order and subsequently transform, by some form of domain nucleation and growth process, into a fully ordered structure which in their work consists of PS spheres on a body-centered cubic lattice. Small-angle scattering data from Hashimoto et al.[30] also indicate that there is a lattice disordering regime near the order−disorder transition. They showed that a structure of PS spheres ordered on a BCC lattice loses long-range translational symmetry as temperature is increased beyond some critical value.

Increasing the exposure to solvent via a slower evaporation rate (parts b−d of Figure 1) results in well-ordered microphase-separated structures with either a vertical-cylinder or in-plane cylinder morphology. On the basis of surface-energy considerations, one can argue that the in-plane morphology is more thermodynamically stable than the vertical morphology. A more sophisticated model would consider variations in volume free energy which would include morphology-dependent chain-stretching contributions.[31,32] These are ignored in the present treatment. Assuming in-plane and vertical morphologies with identical PS/PB volume fractions and identical pure PB surface layers, the total surface energy per unit volume of specimen for the vertical morphology, $G_v$, is

$$G_v = [2\pi rtN_v + 2\pi r^2 N_v]\gamma_{PB/PS} + 2A\gamma_{PB/air}$$

and the total surface energy per unit volume for the in-plane morphology, $G_I$, is

$$G_I = 2\pi rtN_v\gamma_{PB/PS} + 2A\gamma_{PB/air}$$

for a thin-film sample of unit volume $V = At$, where $A$ is the sample top surface area, $t$ is the film thickness, $N_v$ is the number of cylinders per unit volume, $r$ is the cylinder radius, and $\gamma_i$ is the surface tension. The difference $\Delta G = G_v - G_I = 2\pi r^2 N_v \gamma_{PB/PS}$ simply corresponds to the extra energy associated with the cylinder ends in the vertical morphology. The interfacial tension between two incompatible polymers is positive. In the case of PS−PB interfaces, $\gamma_{PS/PB}$ is of order 1.3 mJ/ m$^2$.[33] The vertical-cylinder morphology is thus slightly metastable relative to the in-plane orientation, assuming all other factors are equal. Choosing the unit volume to be $V = At = t^3$, $\Delta G$ can be rewritten as $\Delta G = 2\phi_{PS}\gamma_{PS/PS}/t$, where $\phi_{PS}$ is the volume fraction of the PS cylinders. This form of the relation shows that the relative stability of the in-plane morphology increases with decreasing film thickness.

Under the conditions imposed by solvent casting of thin films, the morphology is influenced both by thermodynamic and kinetic considerations. Diffusion of solvent to the surface can play a controlling role in defining the morphology. In SBS triblock copolymer, toluene diffusion in PS is much lower than that in PB at room temperature.[34] Toluene will thus preferentially escape from a film through the PB phase rather than through the PS phase. Faridi et al.[35] also indicate that the solvent mobility is related not only to the microdomain size and partition ratio but also to the tortuosity associated with the morphology and its relative orientation. Larger values of tortuosity correspond to a longer diffusion path. For example, an in-plane lamellar structure would have a continuous PS layer parallel to the surface which would limit solvent diffusion from interior portion of the specimen to the free surface. Rapid removal of the solvent would tend to align such lamellae perpendicular to the surface in order to provide a continuous higher-solvent diffusivity PB path.[36] In the case of PS cylinders, both vertical and in-plane orientations provide a continuous path for solvent diffusion through the PB phase to the surface. A higher tortuosity can be expected in the in-plane morphology than in the vertical morphology, because a less direct path through the PB phase to the surface is available from the film interior for the in-plane case. Rapid solvent removal would favor alignment of PS cylinders perpendicular to the surface to provide a more effective path for solvent diffusion.

The effect of solvent diffusion on morphological orientation can also be considered in terms of the solvent concentration gradient within the film imposed by different solvent evaporation rates. Henkee et al.[25] argue, for example, that in the case of solvent-cast PS−PB droplets lamellae form with a perpendicular orientation near a free surface due to rapid solvent evaporation there. The lamellae subsequently adopt an in-plane orientation further from the surface where the solvent-evaporation rate is lower and the thermodynamic effects are allowed to exert a controlling influence on the morphology. While no effort was made in the present work to quantitatively measure or control the solvent

concentration or its profile in the thin-film specimen, one can argue that solvent-concentration gradients would be steeper under conditions where solvent is allowed to evaporate relatively quickly. Under such conditions, PS cylinders would grow in the direction of the maximum solvent-concentration gradient and adopt an orientation perpendicular to the plane of the film. In cases where the solvent is extracted more slowly, one would expect smaller gradients in solvent concentration through the film thickness. With less of a kinetic constraint, the subtle thermodynamic effects would then define the PS cylinder orientation to lie in the film plane.

Solvent evaporation also appears to be responsible for the distortion away from pure hexagonal symmetry in the as-cast in-plane cylinder morphology illustrated by Figure 4. This distortion can be largely accounted for by a one-dimensional contraction of the PB matrix along the direction perpendicular to the film plane during the final stages of solvent evaporation. Shibayama et al.[37] and Mori et al.[38] showed using small-angle X-ray scattering that microphase separation occurs in the PS−PI diblock at room temperature at a toluene concentration of approximately 75%. No measurements were made of the solvent concentration at which microphase separation occurs at room temperature for the SBS triblock studied in the present research. One can argue, however, that microphase separation at room temperature would occur with a solvent concentration of at least 75% if not higher because of the particular molecular weight studied. Assuming in the present thin-film case that lateral dimensional changes are largely constrained by contact with the substrate, volume changes associated with solvent evaporation will occur principally in the direction of the film normal. Using the hexagonally arrayed as-cast vertical-cylinder morphology as a reference, the film normal contraction is approximately 60% and the in-plane expansion is approximately 10%. No such distortion is observed in the vertical-cylinder case despite the fact that a similar deswelling procedure phenomena must occur. The PS cylinders play a constraining role in the vertical orientation. They run approximately from the substrate to the free surface. Thickness changes of the film must be accommodated both by the PS and the PB phases in the vertical-cylinder morphology. In contrast, the PS cylinders in the in-plane orientation do not impose a similar constraint. Particularly at solvent concentrations below about 25% where $T_g$ for PS exceeds room temperature, the PS cylinders can almost be thought of as rigid rods in an otherwise pliant and solvated PB matrix.[38,39] Changes in the PB volume from which solvent can escape relatively quickly can be accommodated simply by adjustments in the positions of the PS cylinders. It should be noted that the distorted hexagonal structure of the in-plane cylinders cannot be accounted for by a rotation of the array from a surface normal of [0,1,1̄,0] to [1,1,2̄,0].

Vacuum annealing the as-cast specimens thermally enhances polymer mobility in the absence of solvent and thus provides additional time during which the film morphology can evolve to a more thermodynamically stable state. This research has only examined one specific annealing treatment: 18 h exposure at 140 °C under vacuum. Work reported in the literature by Sakurai et al.[15] used similar annealing conditions but at a slightly higher temperature (155 °C). Annealing the present specimens at 155 °C caused the films to break up and agglomerate into thick islands due to capillary forces acting to minimize the total surface energy of the film including energy associated with the Cu grid/air interface. The mobility of the SBS polymer is apparently sufficient at 140 °C to enable relatively local reconstruction of the film microstructure with little effect on the size and shape of the overall film. There is qualitative evidence that some chemical degradation of the PB block may occur during annealing. For example, a consistent decrease in image contrast was observed upon annealing films cast under very slow solvent-evaporation conditions (Figures 1d and 2d). This effect is due either to an overall thickening of the film or to a decrease in the ability of the $OsO_4$ stain to react with the PB phase because of some thermally induced chemical change. Annealed films could also not be fully redissolved in toluene, suggesting that a portion of the unsaturated carbon bonds in the PB phase form cross-links during the annealing treatment.

Post-evaporation annealing an as-cast specimen increases the interdomain spacing and size of the as-cast morphology independent of the specific film morphology. All observed morphologies, even the disordered ones resulting from fast evaporation, have some characteristic length scale representative of the average spacing between microstructural features (Table 1). The results from the coarsening of the vertical-cylinder morphology (Figure 5) show that both the intercylinder spacing and cylinder radius increase with post-evaporation annealing. This effect can be qualitatively appreciated simply by recognizing that the number of PS cylinders in the two images (parts a and b of Figure 5) are different, yet the specimen image area sampled is the same in the two images. These increases can be attributed to nonequilibrium effects associated with the solvent-evaporation procedure as suggested previously by Shibayama et al.[40] Using small-angle X-ray scattering from a solvated lamellar diblock, Shibayama et al. showed that the interdomain spacing increases with decreasing solvent concentration according to equilibrium thermodynamic considerations.[40] Below a critical solvent concentration (∼25%), however, the interdomain spacing does not increase with further solvent evaporation. They attributed this effect to kinetic limitations where the polymer mobility is too low to enable adjustments to the bulk morphology. Subsequent annealing after solvent evaporation relieves the kinetic constraint, leading to an increase in interdomain spacing consistent with the thermodynamics.

Despite the conclusion that adjustments to intercylinder spacing occur in response to annealing, the present results suggest that the transformation between different morphologies is difficult. This observation is also born out by the more extensive annealing studies of Hajduk et al.[17] and Sakurai et al.[15] There appears to be a relatively large activation barrier associated with nucleation of one type of morphological domain within a parent matrix of another morphology. For example, there is coarsening of microphase-separated features and perhaps traces of cylinder-like features after annealing the fast-evaporated films with the disordered morphology. There is no large-scale transformation into an obviously different and thermodynamically more stable morphology, however. Study of the post-cast-annealed vertical-cylinder morphology leads to a similar finding. Figure 2b shows regions with a modified

microstructure (labeled M) containing elongated features of light contrast that may be a precursor to an in-plane cylinder morphology. These elongated features have similar contrast to the adjacent areas of light contrast on a hexagonal array—presumably the vertical PS cylinders—suggesting that the through-thickness fractions of PS and PB are similar in the two areas. Different mechanisms have been proposed to describe the transformation from lamellae to cylinders and vice versa,[15,17] but a thermally induced orientation change from one orientation of a given morphology to a different orientation of that same morphology has apparently not been considered.

The fact that the duplex morphology (Figure 1c) transforms into a fully in-plane cylinder morphology in response to annealing suggests that the growth of a morphological domain is easier than domain nucleation. The same annealing treatment which is unable to substantially transform the as-cast disordered and vertical-cylinder morphologies is able to fully transform the as-cast duplex morphology. Presumably, the activation energy for domain growth is less than that for nucleation. An energetically less costly growth rate could be a consequence of the morphological structure at the domain boundaries. The plan-view TEM images (Figure 1c) show a typical boundary region between vertical and in-plane cylinder domains. Away from the boundary, the contrast is typical only of either the in-plane or vertical cylinders. Within the boundary, one can see overlapping contrast from both morphologies. With both vertical and in-plane elements present, propagation of a boundary between them may proceed in response to local compression and elongation of individual polymer blocks within the structure.[17]

## Conclusion

This research has studied the development of microphase-separated morphology in solvent-cast thin films of 30 wt % PS SBS triblock copolymer as a function of solvent evaporation rate and post-evaporation annealing and leads to the following conclusions.

(1) Under conditions where the films are exposed to solvent for long periods of time and are subjected to post-evaporation annealing, the morphology consists of PS cylinders lying in the film plane arranged in a hexagonal array within a PB matrix. This morphology is expected from thermodynamic considerations.

(2) Several different film morphologies are observed as a function of solvent evaporation rate. These follow a logical progression from the least to the most ordered as the polymer mobility is increased via slower solvent evaporation. Fast evaporation leads to a microphase-separated morphology where the domains have no long-range order. Slower evaporation rates lead to highly ordered morphologies of PS cylinders in a PB matrix. The cylinders can be oriented either in the plane of the film or perpendicular to it depending on the solvent evaporation rate.

(3) The array of in-plane cylinders in as-cast films shows a distorted hexagonal symmetry which is attributed to an anisotropic contraction of the PB matrix during solvent evaporation.

(4) Post-evaporation annealing either increases the interdomain spacing or transforms the as-cast microstructure into a different microstructure altogether. The coarsening effect is consistent with reports suggesting that kinetic constraints at low solvent concentrations prevent the microstructure from achieving its equilibrium interdomain spacing. Observations concerning morphological transformations suggest that nucleation of domains with a different morphology than the parent morphology is relatively difficult, but once nucleated, growth of new domains proceeds with less of an activation barrier.

**Acknowledgment.** The authors are grateful to the Army Research Office under Grant DAAH04-93-G-0239 and the New Jersey Commission on Science and Technology through the Associated Institutes for Materials Science (AIMS) for financial support. The authors would also like to thank Dr. L. Fetters of Exxon for the GPC analysis, Prof. A. Bose of Stevens for the proton NMR measurements, and Prof. E. L. Thomas of M.I.T. for his many constructive comments on this manuscript.

## References and Notes

(1) Bates, F. S.; Fredrickson, G. *Annu. Rev. Phys. Chem.* **1990**, *41*, 525.
(2) Helfand, E.; Wasserman, Z. R. In *Developments in Block Copolymers*; Goodman, I., Ed.; Applied Science Publishers: London, 1982; pp 99−125.
(3) Richards, R. W. In *Multicomponent Polymer Systems*; Miles, I. S., Rostami, S., Eds.; John Wiley: New York, 1992; p 103.
(4) Thomas, E. L.; Lescanec, R. L. In *Self-Order and Form in Polymeric Materials*; Keller, A., Warner, M., Windle, A. H., Eds.; Chapman and Hall: London, 1995l pp 147−164.
(5) Schulz, M. F.; Bates, F. S. In *Physical Properties of Polymers Handbook*; Mark, J. E., Ed.; AIP Press: New York, 1996; pp 427−433.
(6) Gallot, B. R. M. *Adv. Polym. Sci.* **1978**, *29*, 85.
(7) Meier, D. J. *J. Polym. Sci.* **1969**, *26*, 81.
(8) Helfand, E.; Wasserman, Z. R. *Macromolecules* **1976**, *9*, 879.
(9) Leibler, L. *Macromolecules* **1980**, *13*, 1602.
(10) Thomas, E. L.; Anderson, D.; Henkee, C.; Hoffman, D. *Nature* **1988**, 334, *18*, 598.
(11) Hasegawa, H.; Tanaka, H.; Yamasaki, K.; Hashimoto, T. *Macromolecules* **1987**, *20*, 1651.
(12) Hajduk, D. A.; Harper, P. E.; Gruner, S. M.; Honeker, C. C.; Kim, G.; Thomas, E. L.; Fetters, L. J. *Macromolecules* **1994**, *27*, 4063.
(13) Hashimoto, T.; Kowsaka, T.; Shibayama, M.; Kawai, H. *Macromolecules* **1986**, *19*, 754.
(14) Harkless, C. R.; Singh, M. A.; Nagler, S. E.; Stevenson, G. B.; Jordan-Sweet, J. L. *Phys. Rev. Lett.* **1990**, *64*, 2285.
(15) Sakurai, S.; Kawada, H.; Hashimoto, T.; Fetters, L. J. *Macromolecules* **1993**, *26*, 5796.
(16) Hamley, I. W.; Koppi, K. A.; Rosedale, J. H.; Bates, F. S.; Almdal, K.; Mortenson, K. *Macromolecules* **1993**, *26*, 5959.
(17) Hajduk, D. A.; Gruner, S. M.; Rangarajan, P.; Register, R.; Fetters, L. J.; Honeker, C.; Albalak, R. J.; Thomas, E. L. *Macromolecules* **1994**, *27*, 490.
(18) Paul, D. R. In *Polymer Blends*; Paul, D. R., Newman, S., Eds.; Academic Press: London, 1978; pp 35−62.
(19) Favis, B. D. *Can. J. Chem. Eng.* **1991**, *69*, 619.
(20) Pocius, A. V. In *Physical Properties of Polymers Handbook*; Mark, J., Ed.; AIP Press: New York, 1996; pp 363−369.
(21) Mansky, P.; Harrison, C. K.; Chaikin, P. M.; Register, R. A.; Yao, N. *Appl. Phys. Lett.* **1996**, *68*, 2586.
(22) Mansky, P.; Chaikin, P.; Thomas, E. L. *J. Mater. Sci.* **1995**, *30*, 1987.
(23) Morkved, T. L.; Wiltzius, P.; Jaeger, H. M.; Grier, D. G.; Witten, T. A. *Appl. Phys. Lett.* **1994**, *64*, 422.
(24) Park, M.; Harrison, C.; Chaikin, P. M.; Register, R. A.; Adamson, D. H. *Science* **1997**, *276*, 1401.
(25) Henkee, C.; Thomas, E. L.; Fetters, L. J. *J. Mater. Sci.* **1988**, *23*, 1685.
(26) Radzilowski, L. H.; Carvalho, B. L.; Thomas, E. L. *J. Polym. Sci.* **1996**, *34*, 3081.
(27) Helfand, E.; Wasserman, Z. R. *Macromolecules* **1980**, *13*, 994.
(28) Lu, Q. M.; Libera, M. *J. Appl. Phys.* **1995**, *77*, 517.
(29) Aggarwal, S. *Polymer* **1976**, *17*, 938.
(30) Hashimoto, T.; Shibayama, M.; Kawai, H.; Watanabe, H.; Kotaka, T. *Macromolecules* **1983**, *16*, 361.
(31) Walton, D. G.; Kellogg, G. J.; Mayes, A. M.; Lambooy, P.; Russell, T. P. *Macromolecules* **1994**, *27*, 6225.

(32) Liu, Y.; Rafailovich, M.; Sokolov, J.; Schwarz, S. A.; Bahal, S. *Macromolecules* **1996**, *29*, 899.
(33) Wu, S. *Polym. Eng. Sci.* **1987**, *25*, 335.
(34) Hadj-Rhomdhane, I. Polymer−solvent diffusion and equilibrium parameters by inverse-gas−liquid chromatography, Ph.D. Thesis in Chemical Engineering, Penn State University, 1994.
(35) Faridi, D.; Duda, J.; Hadj-Rhomdhane, I. *Ind. Eng. Chem. Res.* **1995**, *34*, 3556.
(36) Turturro, A.; Gattiglia, E.; Vacca, P.; Viola, G. *Polymer* **1995**, *36*, 3987.
(37) Shibayama, M.; Hashimoto, T.; Hasegawa, H.; Kawai, H. *Macromolecules* **1983**, *16*, 1427.
(38) Mori, K.; Hasegawa, H.; Hashimoto, T. *Polymer* **1990**, *31*, 2368.
(39) Plazek, D.; Ngai, K. In *Physical Properties of Polymers Handbook*; Mark, J., Ed.; AIP Press: New York, 1996; pp 139−159.
(40) Shibayama, M.; Hashimoto, T.; Kawai, H. *Macromolecules* **1983**, *16*, 1434.

MA971349I